

Measurement of the Born cross sections for $e^+e^- \rightarrow \eta'\pi^+\pi^-$ at center-of-mass energies between 2.00 and 3.08 GeV

M. Ablikim¹, M. N. Achasov^{10,c}, P. Adlarson⁶⁷, S. Ahmed¹⁵, M. Albrecht⁴, R. Aliberti²⁸, A. Amoroso^{66a,66c}, Q. An^{63,50}, Anita²¹, X. H. Bai⁵⁷, Y. Bai⁴⁹, O. Bakina²⁹, R. Baldini Ferroli^{23a}, I. Balossino²⁴, Y. Ban^{39,k}, K. Begzsuren²⁶, N. Berger²⁸, M. Bertani^{23a}, D. Bettoni^{24a}, F. Bianchi^{66a,66c}, J. Biernat⁶⁷, J. Bloms⁶⁰, A. Bortone^{66a,66c}, I. Boyko²⁹, R. A. Briere⁵, H. Cai⁶⁸, X. Cai^{1,50}, A. Calcaterra^{23a}, G. F. Cao^{1,55}, N. Cao^{1,55}, S. A. Cetin^{54a}, J. F. Chang^{1,50}, W. L. Chang^{1,55}, G. Chelkov^{29,b}, D. Y. Chen⁶, G. Chen¹, H. S. Chen^{1,55}, M. L. Chen^{1,50}, S. J. Chen³⁶, X. R. Chen²⁵, Y. B. Chen^{1,50}, Z. J. Chen^{20,l}, W. S. Cheng^{66c}, G. Cibinetto^{24a}, F. Cossio^{66c}, X. F. Cui³⁷, H. L. Dai^{1,50}, X. C. Dai^{1,55}, A. Dbeyssi¹⁵, R. E. de Boer⁴, D. Dedovich²⁹, Z. Y. Deng¹, A. Denig²⁸, I. Denysenko²⁹, M. Destefanis^{66a,66c}, F. De Mori^{66a,66c}, Y. Ding³⁴, C. Dong³⁷, J. Dong^{1,50}, L. Y. Dong^{1,55}, M. Y. Dong^{1,50,55}, X. Dong⁶⁸, S. X. Du⁷¹, J. Fang^{1,50}, S. S. Fang^{1,55}, Y. Fang¹, R. Farinelli^{24a}, L. Fava^{66b,66c}, F. Feldbauer⁴, G. Felici^{23a}, C. Q. Feng^{63,50}, M. Fritsch⁴, C. D. Fu¹, Y. Fu¹, Y. Gao^{39,k}, Y. Gao⁶⁴, Y. Gao^{63,50}, Y. G. Gao⁶, I. Garzia^{24a,24b}, E. M. Gersabeck⁵⁸, A. Gilman⁵⁹, K. Goetzen¹¹, L. Gong³⁴, W. X. Gong^{1,50}, W. Gradl²⁸, M. Greco^{66a,66c}, L. M. Gu³⁶, M. H. Gu^{1,50}, S. Gu², Y. T. Gu¹³, C. Y. Guan^{1,55}, A. Q. Guo²², L. B. Guo³⁵, R. P. Guo⁴¹, Y. P. Guo²⁸, Y. P. Guo^{9,h}, A. Guskov²⁹, T. T. Han⁴², X. Q. Hao¹⁶, F. A. Harris⁵⁶, K. L. He^{1,55}, F. H. Heinsius⁴, C. H. Heinz²⁸, T. Held⁴, Y. K. Heng^{1,50,55}, C. Herold⁵², M. Himmelreich^{11,f}, T. Holtmann⁴, Y. R. Hou⁵⁵, Z. L. Hou¹, H. M. Hu^{1,55}, J. F. Hu^{48,m}, T. Hu^{1,50,55}, Y. Hu¹, G. S. Huang^{63,50}, L. Q. Huang⁶⁴, X. T. Huang⁴², Y. P. Huang¹, Z. Huang^{39,k}, N. Huesken⁶⁰, T. Hussain⁶⁵, W. Ikegami Andersson⁶⁷, W. Imoehl²², M. Irshad^{63,50}, S. Jaeger⁴, S. Janchiv^{26,j}, Q. Ji¹, Q. P. Ji¹⁶, X. B. Ji^{1,55}, X. L. Ji^{1,50}, H. B. Jiang⁴², X. S. Jiang^{1,50,55}, X. Y. Jiang³⁷, J. B. Jiao⁴², Z. Jiao¹⁸, S. Jin³⁶, Y. Jin⁵⁷, T. Johansson⁶⁷, N. Kalantar-Nayestanaki³¹, X. S. Kang³⁴, R. Kappert³¹, M. Kavatsyuk³¹, B. C. Ke^{44,1}, I. K. Keshk⁴, A. Khoukaz⁶⁰, P. Kiese²⁸, R. Kiuchi¹, R. Kliemt¹¹, L. Koch³⁰, O. B. Kolcu^{54a,e}, B. Kopf⁴, M. Kuemmel⁴, M. Kuessner⁴, A. Kupsc⁶⁷, M. G. Kurth^{1,55}, W. Kühn³⁰, J. J. Lane⁵⁸, J. S. Lange³⁰, P. Larin¹⁵, L. Lavezzi^{66a,66c}, Z. H. Lei^{63,50}, H. Leithoff²⁸, M. Lellmann²⁸, T. Lenz²⁸, C. Li⁴⁰, C. H. Li³³, Cheng Li^{63,50}, D. M. Li⁷¹, F. Li^{1,50}, G. Li¹, H. Li⁴⁴, H. Li^{63,50}, H. B. Li^{1,55}, H. J. Li^{9,h}, J. L. Li⁴², J. Q. Li⁴, Ke Li¹, L. K. Li¹, Lei Li³, P. L. Li^{63,50}, P. R. Li³², S. Y. Li⁵³, W. D. Li^{1,55}, W. G. Li¹, X. H. Li^{63,50}, X. L. Li⁴², Z. Y. Li⁵¹, H. Liang^{63,50}, H. Liang^{1,55}, Y. F. Liang⁴⁶, Y. T. Liang²⁵, L. Z. Liao^{1,55}, J. Libby²¹, C. X. Lin⁵¹, B. J. Liu¹, C. X. Liu¹, D. Liu^{63,50}, F. H. Liu⁴⁵, Fang Liu¹, Feng Liu⁶, H. B. Liu¹³, H. M. Liu^{1,55}, Huanhuan Liu¹, Huihui Liu¹⁷, J. B. Liu^{63,50}, J. Y. Liu^{1,55}, K. Liu¹, K. Y. Liu³⁴, Ke Liu⁶, L. Liu^{63,50}, M. H. Liu^{9,h}, Q. Liu⁵⁵, S. B. Liu^{63,50}, Shuai Liu⁴⁷, T. Liu^{1,55}, W. M. Liu^{63,50}, X. Liu³², Y. B. Liu³⁷, Z. A. Liu^{1,50,55}, Z. Q. Liu⁴², X. C. Lou^{1,50,55}, F. X. Lu¹⁶, H. J. Lu¹⁸, J. D. Lu^{1,55}, J. G. Lu^{1,50}, X. L. Lu¹, Y. Lu¹, Y. P. Lu^{1,50}, C. L. Luo³⁵, M. X. Luo⁷⁰, P. W. Luo⁵¹, T. Luo^{9,h}, X. L. Luo^{1,50}, S. Lusso^{66c}, X. R. Lyu⁵⁵, F. C. Ma³⁴, H. L. Ma¹, L. L. Ma⁴², M. M. Ma^{1,55}, Q. M. Ma¹, R. Q. Ma^{1,55}, R. T. Ma⁵⁵, X. N. Ma³⁷, X. X. Ma^{1,55}, X. Y. Ma^{1,50}, F. E. Maas¹⁵, M. Maggiora^{66a,66c}, S. Maldaner²⁸, S. Malde⁶¹, Q. A. Malik⁶⁵, A. Mangoni^{23b}, Y. J. Mao^{39,k}, Z. P. Mao¹, S. Marcello^{66a,66c}, Z. X. Meng⁵⁷, J. G. Messchendorp³¹, G. Mezzadri^{24a}, T. J. Min³⁶, R. E. Mitchell²², X. H. Mo^{1,50,55}, Y. J. Mo⁶, N. Yu. Muchnoi^{10,c}, H. Muramatsu⁵⁹, S. Nakhoul^{11,f}, Y. Nefedov²⁹, F. Nerling^{11,f}, I. B. Nikolaev^{10,c}, Z. Ning^{1,50}, S. Nisar^{8,i}, S. L. Olsen⁵⁵, Q. Ouyang^{1,50,55}, S. Pacetti^{23b,23c}, X. Pan^{9,h}, Y. Pan⁵⁸, A. Pathak¹, P. Patteri^{23a}, M. Pelizzaeus⁴, H. P. Peng^{63,50}, K. Peters^{11,f}, J. Pettersson⁶⁷, J. L. Ping³⁵, R. G. Ping^{1,55}, A. Pitka⁴, R. Poling⁵⁹, V. Prasad^{63,50}, H. Qi^{63,50}, H. R. Qi⁵³, K. H. Qi²⁵, M. Qi³⁶, T. Y. Qi², T. Y. Qi⁹, S. Qian^{1,50}, W.-B. Qian⁵⁵, Z. Qian⁵¹, C. F. Qiao⁵⁵, L. Q. Qin¹², X. S. Qin⁴, Z. H. Qin^{1,50}, J. F. Qiu¹, S. Q. Qu³⁷, K. H. Rashid⁶⁵, K. Ravindran²¹, C. F. Redmer²⁸, A. Rivetti^{66c}, V. Rodin³¹, M. Rolo^{66c}, G. Rong^{1,55}, Ch. Rosner¹⁵, M. Rump⁶⁰, H. S. Sang⁶³, A. Sarantsev^{29,d}, Y. Schelhaas²⁸, C. Schnier⁴, K. Schoenning⁶⁷, M. Scodreggio^{24a}, D. C. Shan⁴⁷, W. Shan¹⁹, X. Y. Shan^{63,50}, M. Shao^{63,50}, C. P. Shen⁹, P. X. Shen³⁷, X. Y. Shen^{1,55}, H. C. Shi^{63,50}, R. S. Shi^{1,55}, X. Shi^{1,50}, X. D. Shi^{63,50}, W. M. Song^{27,1}, Y. X. Song^{39,k}, S. Sosio^{66a,66c}, S. Spataro^{66a,66c}, K. X. Su⁶⁸, F. F. Sui⁴², G. X. Sun¹, H. K. Sun¹, J. F. Sun¹⁶, L. Sun⁶⁸, S. S. Sun^{1,55}, T. Sun^{1,55}, W. Y. Sun³⁵, X. Sun^{20,l}, Y. J. Sun^{63,50}, Y. K. Sun^{63,50}, Y. Z. Sun¹, Z. T. Sun¹, Y. H. Tan⁶⁸, Y. X. Tan^{63,50}, C. J. Tang⁴⁶, G. Y. Tang¹, J. Tang⁵¹, J. X. Teng^{63,50}, V. Thoren⁶⁷, I. Uman^{54b}, C. W. Wang³⁶, D. Y. Wang^{39,k}, H. P. Wang^{1,55}, K. Wang^{1,50}, L. L. Wang¹, M. Wang⁴², M. Z. Wang^{39,k}, Meng Wang^{1,55}, W. H. Wang⁶⁸, W. P. Wang^{63,50}, X. Wang^{39,k}, X. F. Wang³², X. L. Wang^{9,h}, Y. Wang⁵¹, Y. Wang^{63,50}, Y. D. Wang³⁸, Y. F. Wang^{1,50,55}, Y. Q. Wang¹, Z. Wang^{1,50}, Z. Y. Wang¹, Ziyi Wang⁵⁵, Zongyuan Wang^{1,55}, D. H. Wei¹², P. Weidenkaff²⁸, F. Weidner⁶⁰, S. P. Wen¹, D. J. White⁵⁸, U. Wiedner⁴, G. Wilkinson⁶¹, M. Wolke⁶⁷, L. Wollenberg⁴, J. F. Wu^{1,55}, L. H. Wu¹, L. J. Wu^{1,55}, X. Wu^{9,h}, Z. Wu^{1,50}, L. Xia^{63,50}, H. Xiao^{9,h}, S. Y. Xiao¹, Y. J. Xiao^{1,55}, Z. J. Xiao³⁵, X. H. Xie^{39,k}

Y. G. Xie^{1,50}, Y. H. Xie⁶, T. Y. Xing^{1,55}, G. F. Xu¹, J. J. Xu³⁶, Q. J. Xu¹⁴, W. Xu^{1,55}, X. P. Xu⁴⁷, F. Yan^{9,h},
 L. Yan^{66a,66c}, L. Yan^{9,h}, W. B. Yan^{63,50}, W. C. Yan⁷¹, Xu Yan⁴⁷, H. J. Yang^{43,g}, H. X. Yang¹, L. Yang⁴⁴,
 R. X. Yang^{63,50}, S. L. Yang⁵⁵, S. L. Yang^{1,55}, Y. H. Yang³⁶, Y. X. Yang¹², Yifan Yang^{1,55}, Zhi Yang²⁵,
 M. Ye^{1,50}, M. H. Ye⁷, J. H. Yin¹, Z. Y. You⁵¹, B. X. Yu^{1,50,55}, C. X. Yu³⁷, G. Yu^{1,55}, J. S. Yu^{20,l}, T. Yu⁶⁴,
 C. Z. Yuan^{1,55}, L. Yuan², W. Yuan^{66a,66c}, X. Q. Yuan^{39,k}, Y. Yuan¹, Z. Y. Yuan⁵¹, C. X. Yue³³, A. Yuncu^{54a,a},
 A. A. Zafar⁶⁵, Y. Zeng^{20,l}, B. X. Zhang¹, Guangyi Zhang¹⁶, H. Zhang⁶³, H. H. Zhang⁵¹, H. Y. Zhang^{1,50},
 J. J. Zhang⁴⁴, J. L. Zhang⁶⁹, J. Q. Zhang⁴, J. Q. Zhang³⁵, J. W. Zhang^{1,50,55}, J. Y. Zhang¹, J. Z. Zhang^{1,55},
 Jianyu Zhang^{1,55}, Jiawei Zhang^{1,55}, Lei Zhang³⁶, S. Zhang⁵¹, S. F. Zhang³⁶, Shulei Zhang^{20,l}, X. D. Zhang³⁸,
 X. Y. Zhang⁴², Y. Zhang⁶¹, Y. H. Zhang^{1,50}, Y. T. Zhang^{63,50}, Yan Zhang^{63,50}, Yao Zhang¹, Yi Zhang^{9,h},
 Z. H. Zhang⁶, Z. Y. Zhang⁶⁸, G. Zhao¹, J. Zhao³³, J. Y. Zhao^{1,55}, J. Z. Zhao^{1,50}, Lei Zhao^{63,50}, Ling Zhao¹,
 M. G. Zhao³⁷, Q. Zhao¹, S. J. Zhao⁷¹, Y. B. Zhao^{1,50}, Y. X. Zhao²⁵, Z. G. Zhao^{63,50}, A. Zhemchugov^{29,b},
 B. Zheng⁶⁴, J. P. Zheng^{1,50}, Y. Zheng^{39,k}, Y. H. Zheng⁵⁵, B. Zhong³⁵, C. Zhong⁶⁴, L. P. Zhou^{1,55},
 Q. Zhou^{1,55}, X. Zhou⁶⁸, X. K. Zhou⁵⁵, X. R. Zhou^{63,50}, A. N. Zhu^{1,55}, J. Zhu³⁷, K. Zhu¹, K. J. Zhu^{1,50,55},
 S. H. Zhu⁶², T. J. Zhu⁶⁹, W. J. Zhu³⁷, X. L. Zhu⁵³, Y. C. Zhu^{63,50}, Z. A. Zhu^{1,55}, B. S. Zou¹, J. H. Zou¹

(BESIII Collaboration)

¹*Institute of High Energy Physics, Beijing 100049, People's Republic of China*

²*Beihang University, Beijing 100191, People's Republic of China*

³*Beijing Institute of Petrochemical Technology, Beijing 102617, People's Republic of China*

⁴*Bochum Ruhr-University, D-44780 Bochum, Germany*

⁵*Carnegie Mellon University, Pittsburgh, Pennsylvania 15213, USA*

⁶*Central China Normal University, Wuhan 430079, People's Republic of China*

⁷*China Center of Advanced Science and Technology, Beijing 100190, People's Republic of China*

⁸*COMSATS University Islamabad, Lahore Campus, Defence Road, Off Raiwind Road, 54000 Lahore, Pakistan*

⁹*Fudan University, Shanghai 200443, People's Republic of China*

¹⁰*G.I. Budker Institute of Nuclear Physics SB RAS (BINP), Novosibirsk 630090, Russia*

¹¹*GSI Helmholtzcentre for Heavy Ion Research GmbH, D-64291 Darmstadt, Germany*

¹²*Guangxi Normal University, Guilin 541004, People's Republic of China*

¹³*Guangxi University, Nanning 530004, People's Republic of China*

¹⁴*Hangzhou Normal University, Hangzhou 310036, People's Republic of China*

¹⁵*Helmholtz Institute Mainz, Johann-Joachim-Becher-Weg 45, D-55099 Mainz, Germany*

¹⁶*Henan Normal University, Xinxiang 453007, People's Republic of China*

¹⁷*Henan University of Science and Technology, Luoyang 471003, People's Republic of China*

¹⁸*Huangshan College, Huangshan 245000, People's Republic of China*

¹⁹*Hunan Normal University, Changsha 410081, People's Republic of China*

²⁰*Hunan University, Changsha 410082, People's Republic of China*

²¹*Indian Institute of Technology Madras, Chennai 600036, India*

²²*Indiana University, Bloomington, Indiana 47405, USA*

^{23a}*INFN Laboratori Nazionali di Frascati, I-00044 Frascati, Italy*

^{23b}*INFN Sezione di Perugia, I-06100 Perugia, Italy*

^{23c}*University of Perugia, I-06100, Perugia, Italy*

^{24a}*INFN Sezione di Ferrara, I-44122 Ferrara, Italy*

^{24b}*University of Ferrara, I-44122, Ferrara, Italy*

²⁵*Institute of Modern Physics, Lanzhou 730000, People's Republic of China*

²⁶*Institute of Physics and Technology, Peace Ave. 54B, Ulaanbaatar 13330, Mongolia*

²⁷*Jilin University, Changchun 130012, People's Republic of China*

²⁸*Johannes Gutenberg University of Mainz, Johann-Joachim-Becher-Weg 45, D-55099 Mainz, Germany*

²⁹*Joint Institute for Nuclear Research, 141980 Dubna, Moscow region, Russia*

³⁰*Justus-Liebig-Universitaet Giessen, II. Physikalisches Institut, Heinrich-Buff-Ring 16, D-35392 Giessen, Germany*

³¹*KVI-CART, University of Groningen, NL-9747 AA Groningen, The Netherlands*

³²*Lanzhou University, Lanzhou 730000, People's Republic of China*

³³*Liaoning Normal University, Dalian 116029, People's Republic of China*

³⁴*Liaoning University, Shenyang 110036, People's Republic of China*

³⁵*Nanjing Normal University, Nanjing 210023, People's Republic of China*

- ³⁶Nanjing University, Nanjing 210093, People's Republic of China
- ³⁷Nankai University, Tianjin 300071, People's Republic of China
- ³⁸North China Electric Power University, Beijing 102206, People's Republic of China
- ³⁹Peking University, Beijing 100871, People's Republic of China
- ⁴⁰Qufu Normal University, Qufu 273165, People's Republic of China
- ⁴¹Shandong Normal University, Jinan 250014, People's Republic of China
- ⁴²Shandong University, Jinan 250100, People's Republic of China
- ⁴³Shanghai Jiao Tong University, Shanghai 200240, People's Republic of China
- ⁴⁴Shanxi Normal University, Linfen 041004, People's Republic of China
- ⁴⁵Shanxi University, Taiyuan 030006, People's Republic of China
- ⁴⁶Sichuan University, Chengdu 610064, People's Republic of China
- ⁴⁷Soochow University, Suzhou 215006, People's Republic of China
- ⁴⁸South China Normal University, Guangzhou 510006, People's Republic of China
- ⁴⁹Southeast University, Nanjing 211100, People's Republic of China
- ⁵⁰State Key Laboratory of Particle Detection and Electronics,
Beijing 100049, Hefei 230026, People's Republic of China
- ⁵¹Sun Yat-Sen University, Guangzhou 510275, People's Republic of China
- ⁵²Suranaree University of Technology, University Avenue 111, Nakhon Ratchasima 30000, Thailand
- ⁵³Tsinghua University, Beijing 100084, People's Republic of China
- ^{54a}Turkish Accelerator Center Particle Factory Group, Istanbul Bilgi University, 34060 Eyup, Istanbul, Turkey
- ^{54b}Near East University, Nicosia, North Cyprus, Mersin 10, Turkey
- ⁵⁵University of Chinese Academy of Sciences, Beijing 100049, People's Republic of China
- ⁵⁶University of Hawaii, Honolulu, Hawaii 96822, USA
- ⁵⁷University of Jinan, Jinan 250022, People's Republic of China
- ⁵⁸University of Manchester, Oxford Road, Manchester, M13 9PL, United Kingdom
- ⁵⁹University of Minnesota, Minneapolis, Minnesota 55455, USA
- ⁶⁰University of Muenster, Wilhelm-Klemm-Str. 9, 48149 Muenster, Germany
- ⁶¹University of Oxford, Keble Rd, Oxford, UK OX13RH
- ⁶²University of Science and Technology Liaoning, Anshan 114051, People's Republic of China
- ⁶³University of Science and Technology of China, Hefei 230026, People's Republic of China
- ⁶⁴University of South China, Hengyang 421001, People's Republic of China
- ⁶⁵University of the Punjab, Lahore-54590, Pakistan
- ^{66a}University of Turin, I-10125, Turin, Italy
- ^{66b}University of Eastern Piedmont, I-15121, Alessandria, Italy
- ^{66c}INFN, I-10125, Turin, Italy
- ⁶⁷Uppsala University, Box 516, SE-75120 Uppsala, Sweden
- ⁶⁸Wuhan University, Wuhan 430072, People's Republic of China
- ⁶⁹Xinyang Normal University, Xinyang 464000, People's Republic of China
- ⁷⁰Zhejiang University, Hangzhou 310027, People's Republic of China
- ⁷¹Zhengzhou University, Zhengzhou 450001, People's Republic of China
- ^aAlso at Bogazici University, 34342 Istanbul, Turkey
- ^bAlso at the Moscow Institute of Physics and Technology, Moscow 141700, Russia
- ^cAlso at the Novosibirsk State University, Novosibirsk, 630090, Russia
- ^dAlso at the NRC "Kurchatov Institute", PNPI, 188300, Gatchina, Russia
- ^eAlso at Istanbul Arel University, 34295 Istanbul, Turkey
- ^fAlso at Goethe University Frankfurt, 60323 Frankfurt am Main, Germany
- ^gAlso at Key Laboratory for Particle Physics, Astrophysics and Cosmology, Ministry of Education; Shanghai Key Laboratory for Particle Physics and Cosmology; Institute of Nuclear and Particle Physics, Shanghai 200240, People's Republic of China
- ^hAlso at Key Laboratory of Nuclear Physics and Ion-beam Application (MOE) and Institute of Modern Physics, Fudan University, Shanghai 200443, People's Republic of China
- ⁱAlso at Harvard University, Department of Physics, Cambridge, MA, 02138, USA
- ^jCurrently at: Institute of Physics and Technology, Peace Ave.54B, Ulaanbaatar 13330, Mongolia

^kAlso at State Key Laboratory of Nuclear Physics and Technology,
Peking University, Beijing 100871, People's Republic of China

^lSchool of Physics and Electronics, Hunan University, Changsha 410082, China

^mAlso at Guangdong Provincial Key Laboratory of Nuclear Science, Institute of
Quantum Matter, South China Normal University, Guangzhou 510006, China

(Dated: November 9, 2021)

The Born cross sections for the process $e^+e^- \rightarrow \eta'\pi^+\pi^-$ at different center-of-mass energies between 2.00 and 3.08 GeV are reported with improved precision from an analysis of data samples collected with the BESIII detector operating at the BEPCII storage ring. An obvious structure is observed in the Born cross section line shape. Fit as a Breit-Wigner resonance, it has a statistical significance of 6.3σ and a mass and width of $M = (2111 \pm 43 \pm 25) \text{ MeV}/c^2$ and $\Gamma = (135 \pm 34 \pm 30) \text{ MeV}$, where the uncertainties are statistical and systematic, respectively. These measured resonance parameters agree with the measurements of BABAR in $e^+e^- \rightarrow \eta'\pi^+\pi^-$ and BESIII in $e^+e^- \rightarrow \omega\pi^0$ within two standard deviations.

PACS numbers:

I. INTRODUCTION

Low energy e^+e^- collision experiments, where ρ , ω and ϕ resonances as well as their excited states are produced copiously, offer an ideal test-bed to thoroughly investigate the properties of these resonances. Many experimental results regarding these states have been summarized in the Particle Data Group (PDG) review [1]. Still, the properties of some states are still ambiguous. Notably, the status of the $\rho(2000)$, $\rho(2150)$, and $\rho(2270)$ states is unclear, due to insufficient experimental information. The $\rho(2000)$ was found in $p\bar{p}$ collisions [2–6], and it was explained as a radial excitation of the $\rho(1700)$ [6] or a mixed state with a significant 3D_1 component [7]. The $\rho(2150)$ was initially regarded as a $^2^3D_1$ state [8], but later was considered to be a 4^3S_1 state [9–13]. The $\rho(2270)$ was first observed in photo-production [14] and categorized as a 3^3D_1 state [12]. There are no published results on $\rho(2000)$ and $\rho(2270)$ from e^+e^- collision experiments. The $\rho(2150)$ has been widely studied in e^+e^- , $p\bar{p}$, s -channel $N\bar{N}$ and πp collision experiments, but inconsistencies in the measured masses and widths make the $\rho(2150)$ more controversial.

According to the vector meson dominance model [15], the isovector part of the electromagnetic current in the positive G-parity process $e^+e^- \rightarrow \eta'\pi^+\pi^-$ allows direct production of ρ -like states. Therefore this process can be used to extract the resonance parameters of the ρ -like states. The BABAR Collaboration has measured the Born cross section line shape of $e^+e^- \rightarrow \eta'\pi^+\pi^-$ at center-of-mass (c.m.) energies (\sqrt{s}) from 1.58 to 3.42 GeV with the initial state radiation (ISR) technique. A resonance-like structure around 2.1 GeV/ c^2 reported by BABAR could be interpreted as the $\rho(2150)$ [16].

By using 19 data sets taken at \sqrt{s} between 2.00 and 3.08 GeV, the BESIII Collaboration recently reported a $J^{PC} = 1^{--}$ vector state, $Y(2040)$, in $e^+e^- \rightarrow \omega\pi^0$ [17] with a mass and width of $(2034 \pm 13 \pm 9) \text{ MeV}/c^2$ and $(234 \pm 30 \pm 25) \text{ MeV}$, respectively. Here, we report the

Born cross sections for $e^+e^- \rightarrow \eta'\pi^+\pi^-$ based on the same data sets. By fitting to these cross sections, we measure the parameters of the possible ρ -like resonances.

II. BESIII AND MONTE CARLO SIMULATION

BESIII is a general-purpose detector located at the Beijing Electron Positron Collider (BEPCII) [18] and is designed for studies of hadron spectroscopy and τ -charm physics [19, 20]. The cylindrical detector has a geometrical acceptance of 93% of 4π solid angle and consists of four main components:

(i) A small cell, helium-based main drift chamber (MDC) with 43 layers immersed in the 1.0 T magnetic field of a super conducting solenoid. The average single-hit resolution is 135 μm , and the charged particle momentum resolution is 0.5% at 1.0 GeV/ c .

(ii) A time-of-flight system (TOF) made from two layers of plastic scintillator, with 88 counters 5 cm thick and 2.4 m long in each layer for the barrel, and 96 fan-shaped counters in each end cap. It provides timing information with a resolution of 68 ps in the barrel and 110 ps in the end caps, which yields 2σ K/π separation at 1.0 GeV/ c .

(iii) An electromagnetic calorimeter (EMC) consisting of 6240 CsI (TI) crystals in a cylindrical barrel and two end caps to measure shower energies. The photon energy resolution at 1.0 GeV is 2.5% in the barrel and 5% in the end caps, while the position resolution is 6 mm and 9 mm for barrel and end caps, respectively.

(iv) A resistive plate chamber (RPC)-based muon chamber (MUC) with nine layers in the barrel and eight layers in the end caps providing 2 cm position resolution.

Monte Carlo (MC) simulations of the full detector, based on GEANT4 [21] simulation software, and the BESIII OBJECT ORIENTED SIMULATION TOOL (BOOST) [22], are used to optimize the event selection

criteria, understand potential backgrounds, and determine the detection efficiency. The BOOST package contains the detector geometry and material description, the detector response and signal digitization models, as well as records of the detector running conditions and performance. Large inclusive MC samples at $\sqrt{s} = 2.1250$ and 2.3960 GeV are generated to estimate potential backgrounds. The processes $e^+e^- \rightarrow e^+e^-, \mu^+\mu^-$ and $\gamma\gamma$ are generated with the Babayaga generator [23], while $e^+e^- \rightarrow$ hadrons and two photon processes are simulated by the LUARLW [24] and BESTWOGAM [25] generators, respectively. Due to the dominance of $\rho\eta'$ in $e^+e^- \rightarrow \eta'\pi^+\pi^-$ process [16], the signal MC is generated with CONEXC [26] as $e^+e^- \rightarrow \rho\eta'$. The cross sections measured by the BABAR experiment [16] are used as initial input. The ISR, vacuum polarization and the angular distributions of the final state have been taken into account in the generator. The wide ρ resonance in the intermediate state is described by the Gounaris-Sakurai (GS) model [27]. The $\eta' \rightarrow \gamma\pi^+\pi^-$ decay is simulated with a model based on the results of the amplitude analysis in Ref. [28], and the $\eta' \rightarrow \eta\pi^+\pi^-$ decay is produced using a phase-space (PHSP) model.

III. DATA ANALYSIS

In this analysis, the η' is reconstructed via the two decay modes $\eta' \rightarrow \eta\pi^+\pi^-$ and $\eta' \rightarrow \gamma\pi^+\pi^-$, which will be referred to as mode I and mode II, respectively. For mode I, the η is reconstructed in the decay $\eta \rightarrow \gamma\gamma$.

Charged tracks are reconstructed using hits in the MDC. Each track is required to be within the polar angle (θ) region $|\cos\theta| < 0.93$ and have a distance of closest approach to the interaction point within ± 10 cm along the beam direction (z -axis) and within 1 cm in the transverse plane. For both modes, it is required that there are exactly four charged tracks with net zero charge. Particle identification (PID) for charged tracks combines the measurements of the specific ionization energy, dE/dx , in the MDC and the flight time in the TOF. The charged track is identified as a pion if the confidence level for the pion hypothesis is greater than those for both the kaon and proton hypotheses.

Showers in the EMC are chosen as photon candidates if they satisfy the following requirements: the deposited energy must be larger than 25 MeV in the barrel region ($|\cos\theta| < 0.80$) and 50 MeV in the end cap ($0.86 < |\cos\theta| < 0.92$). To suppress electronic noise and showers unrelated to the event, the EMC time deviation from the event start time is required to be within (0,700) ns. For mode I (mode II), it is required that there are at least two (one) photons.

A vertex fit is imposed on the selected charged tracks to ensure that they originate from the same interaction point. To improve momentum resolution and to suppress

background, a four-constraint (4C) kinematic fit imposing energy-momentum conservation under the hypotheses of $e^+e^- \rightarrow \gamma\gamma\pi^+\pi^-\pi^+\pi^-$ and $e^+e^- \rightarrow \gamma\pi^+\pi^-\pi^+\pi^-$ is employed on the selected candidates for mode I and mode II, respectively. For events with additional photon(s), the combination with the smallest χ_{4C}^2 is retained. Based on an optimization of $s/\sqrt{s'+b}$ for the requirement on χ_{4C}^2 , where s and $s'+b$ is the number of events in the η' signal region ($(M(\eta\pi^+\pi^-, \gamma\pi^+\pi^-) \in (0.943, 0.973) \text{ GeV}/c^2)$) in signal MC and data, respectively, candidate events with $\chi_{4C}^2 < 100$ ($\chi_{4C}^2 < 50$) for mode I (mode II) are accepted for further analysis. For mode II, to suppress contaminations from $e^+e^- \rightarrow 2(\pi^+\pi^-)$ and $e^+e^- \rightarrow 2(\gamma\pi^+\pi^-)$, two additional 4C kinematic fits under each of these two hypotheses are performed. Events are discarded if the χ_{4C}^2 for either of these fits is less than the signal mode 4C kinematic fit. To further suppress background from $e^+e^- \rightarrow 2(\pi^+\pi^-)$, all photon energies are required to be greater than 0.1 GeV for mode II. For convenience, we take the data set at $\sqrt{s} = 2.1250$ GeV, which has the the largest statistics, as an example in this section. Figure 1 shows the $M(\gamma\gamma)$ distribution of the accepted candidates for $e^+e^- \rightarrow \eta'\pi^+\pi^-$ using mode I. The events in the η mass signal region, $M(\gamma\gamma) \in (0.523, 0.573) \text{ GeV}/c^2$ (the region between two solid blue arrows), are kept for further analysis.

Figure 2 presents the distributions of $M(\eta\pi^+\pi^-)$ for mode I and $M(\gamma\pi^+\pi^-)$ for mode II of the accepted candidates. Clear η' signals are observed. For mode I, the non- η backgrounds in the η mass signal region are examined by the events in the η mass sideband region, which is defined as $M(\gamma\gamma) \in (0.488, 0.513) \cup (0.583, 0.608) \text{ GeV}/c^2$ (the region between two neighboring dashed green arrows in Figure. 1). The resulting $M(\eta\pi^+\pi^-)$ distribution of the η sideband events is shown as the green shaded histogram in Figure. 2(a). Further studies based on the inclusive MC samples show that the dominant backgrounds are $e^+e^- \rightarrow \eta 2(\pi^+\pi^-)|_{\text{non-}\eta'}$ for mode I and $e^+e^- \rightarrow 2(\pi^+\pi^-)$ for mode II. The resulting $M(\eta\pi^+\pi^-, \gamma\pi^+\pi^-)$ distribution of the accepted background events from the inclusive MC samples for mode I and mode II are shown as the magenta histograms of Figure. 2 (a) and (b), respectively. No peaking backgrounds are seen near the η' mass. Therefore, we will fit the $M(\eta\pi^+\pi^-)$ ($M(\gamma\pi^+\pi^-)$) spectra using a smooth background shape to account for the remaining backgrounds in the analysis.

Possible intermediate states in $e^+e^- \rightarrow \eta'\pi^+\pi^-$ are examined by the corresponding Dalitz plots selecting the η' signal region as $M(\eta\pi^+\pi^-, \gamma\pi^+\pi^-) \in (0.943, 0.973) \text{ GeV}/c^2$, shown in Figure 3. After subtracting the non- η' background in the η' sideband region, $M(\eta\pi^+\pi^-, \gamma\pi^+\pi^-) \in (0.918, 0.938) \cup (0.978, 0.998) \text{ GeV}/c^2$, with a weight factor of 0.8. Figure 4 presents the projections of the corresponding Dalitz plots on the $M^2(\pi^+\pi^-)$ axis for two modes. As expected, the dominant component is $e^+e^- \rightarrow \rho\eta'$, and the non- ρ contribution is less than 10%. A fit to the $M(\pi^+\pi^-)$

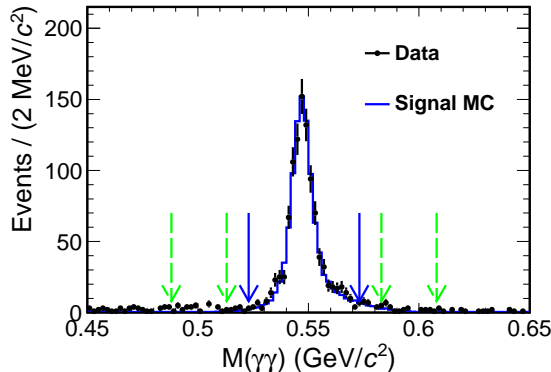


Figure 1: The $M(\gamma\gamma)$ spectrum of the $e^+e^- \rightarrow \eta'\pi^+\pi^-$ candidate events for mode I in data (dots with error bars) and signal MC (histogram) at $\sqrt{s} = 2.1250$ GeV. The region between the two solid blue arrows is the η signal region, while the regions between the pairs of dashed green arrows are the η sideband regions.

in the high-statistics bin at c.m. energy of 2.125 GeV shows that the apparent shift between MC and data of the $\rho(770)$ peak can be explained by interference between $\rho(770)$ and non- $\rho(770)$ process.

IV. BORN CROSS SECTION MEASUREMENT

The Born cross section, σ^B , at each c.m. energy is determined as

$$\sigma^B = \frac{N^{\text{obs}}}{\mathcal{L} \cdot \epsilon \cdot \mathcal{B} \cdot (1 + \delta^r) \cdot \frac{1}{|1 - \Pi|^2}}, \quad (1)$$

where N^{obs} is the signal yield, \mathcal{L} is the integrated luminosity of the data set, ϵ is the detection efficiency, \mathcal{B} is the product of the relevant daughter branching fractions, i.e., $\mathcal{B} = \mathcal{B}(\eta' \rightarrow \eta\pi^+\pi^-) \cdot \mathcal{B}(\eta \rightarrow \gamma\gamma) = 16.8\%$ for mode I and $\mathcal{B} = \mathcal{B}(\eta' \rightarrow \gamma\pi^+\pi^-) = 28.9\%$ for mode II [1]. The factor $(1 + \delta^r)$ is the ISR correction factor and $\frac{1}{|1 - \Pi|^2}$ is the vacuum polarization factor. Both $(1 + \delta^r)$ and $\frac{1}{|1 - \Pi|^2}$ are obtained from MC simulations [29, 30]. To obtain reliable detection efficiencies and ISR factors, the Born cross sections used as input in the generator have been iterated until the product $(1 + \delta^r) \cdot \epsilon$ has converged, defined as an iteration leading to a relative change of less than 1.0%.

The signal yields are obtained from a simultaneous unbinned maximum-likelihood fit to the $M(\eta\pi^+\pi^-)$ and $M(\gamma\pi^+\pi^-)$ spectra at each c.m. energy. The signal is described by a MC-simulated shape convolved with a Gaussian function. The parameters of the Gaussian function are free. Among the different data sets, a common Gaussian convolution is used to compensate for potential differences in calibration and resolution between data and MC simulation. A second-order Chebyshev

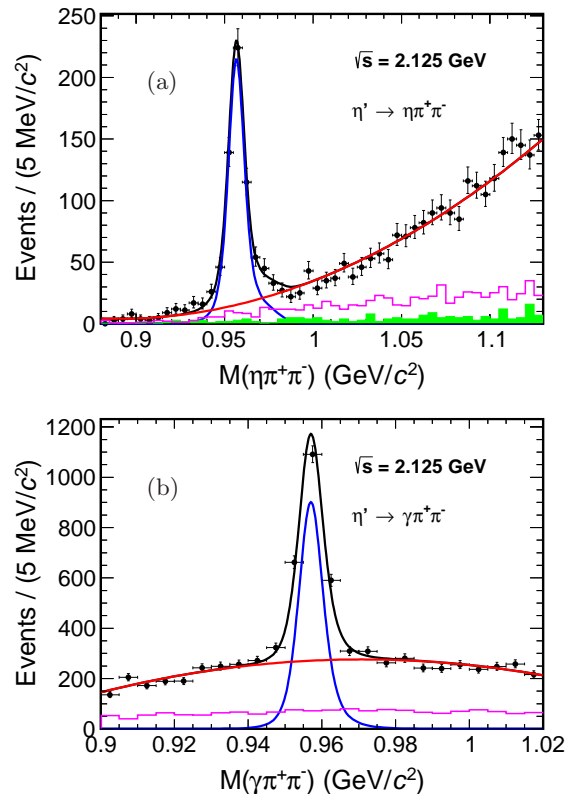


Figure 2: Fits to (a) $M(\eta\pi^+\pi^-)$ and (b) $M(\gamma\pi^+\pi^-)$ for the accepted candidate events in data at $\sqrt{s} = 2.1250$ GeV. Dots with error bars show the data, black lines give the total fit results, blue dotted lines are the signal components, red lines are the smooth backgrounds, and magenta histograms are the inclusive MC samples. The inclusive MC samples are normalized to the data luminosity. The green shaded histogram in (a) shows the events from the η sidebands in data.

polynomial is used to describe the combinatorial background shape. In the fit, the two modes share the same Born cross section, and the expected signal yields are $N^{\text{obs}} = \sigma^B \cdot \mathcal{L} \cdot \epsilon \cdot \mathcal{B} \cdot (1 + \delta^r) \cdot \frac{1}{|1 - \Pi|^2}$. Figure 2 shows the fit result for data taken at $\sqrt{s} = 2.1250$ GeV. Similar combined fits to the two final states are performed for each c.m. energy; the resulting cross sections and related variables are listed in Table I. They are consistent with those from the BABAR experiment [16], as seen in Figure. 5. Independent fits to the $M(\eta\pi^+\pi^-)$ and $M(\gamma\pi^+\pi^-)$ spectra are also performed and the individual signal yields are also summarized in Table I.

By implementing the same strategy described in [31–34], several sources of systematic uncertainty on the measured cross section are considered. These uncertainties for all datasets are summarized in Table II.

The uncertainty in the measurement of the integrated luminosity of the data set has been determined to be 1.0% [35]. The uncertainties of the track reconstruction and PID efficiencies of charged pions have been studied by using a control sample of $e^+e^- \rightarrow K^+K^-\pi^+\pi^-$ [31],

Table I: Summary of the integrated luminosities (\mathcal{L}) [35], observed event yields from independent fit (N^{obs}), detection efficiencies (ϵ), radiative correction factors ($1+\delta^r$), vacuum polarization factors $\frac{1}{|1-\Pi|^2}$, and the obtained Born cross section (σ^B) at different c.m. energies (\sqrt{s}). The first uncertainties for σ^B are statistical and the second are systematic; those for $N^{obs\ I}$ and $N^{obs\ II}$ are statistical only. The symbols of I and II represent the $e^+e^- \rightarrow \eta'\pi^+\pi^-$ processes reconstructed via $\eta' \rightarrow \eta\pi^+\pi^-$ and $\eta' \rightarrow \gamma\pi^+\pi^-$, respectively.

\sqrt{s} (GeV)	\mathcal{L} (pb $^{-1}$)	$N^{obs\ I}$	$N^{obs\ II}$	ϵ^I	ϵ^{II}	$1 + \delta^r$	$\frac{1}{ 1-\Pi ^2}$	σ^B (pb)
2.0000	10.1	35.4 ± 7.5	119.2 ± 16.8	0.157	0.265	0.983	1.037	$144.0 \pm 17.0 \pm 9.7$
2.0500	3.34	23.9 ± 5.5	55.6 ± 10.6	0.167	0.275	0.941	1.038	$229.3 \pm 33.2 \pm 15.7$
2.1000	12.2	58.6 ± 9.1	207.9 ± 19.6	0.166	0.269	0.979	1.039	$200.1 \pm 16.3 \pm 14.1$
2.1250	108.	555.4 ± 27.4	1684.6 ± 58.2	0.160	0.258	1.016	1.039	$191.0 \pm 5.4 \pm 12.7$
2.1500	2.84	8.7 ± 3.7	53.0 ± 9.3	0.154	0.252	1.045	1.040	$184.8 \pm 31.9 \pm 12.5$
2.1750	10.6	43.7 ± 7.7	116.4 ± 15.7	0.159	0.251	1.059	1.040	$137.6 \pm 14.7 \pm 9.1$
2.2000	13.7	36.0 ± 7.6	130.1 ± 16.6	0.155	0.247	1.075	1.040	$108.8 \pm 12.0 \pm 9.3$
2.2324	11.9	35.1 ± 7.4	127.0 ± 15.8	0.156	0.244	1.089	1.041	$122.0 \pm 13.2 \pm 9.9$
2.3094	21.1	45.8 ± 8.2	149.1 ± 17.9	0.153	0.237	1.109	1.041	$83.3 \pm 8.4 \pm 5.6$
2.3864	22.5	57.5 ± 8.8	158.1 ± 17.4	0.152	0.232	1.120	1.041	$87.9 \pm 7.9 \pm 6.3$
2.3960	66.9	167.9 ± 15.2	496.1 ± 31.7	0.156	0.235	1.119	1.041	$89.3 \pm 4.7 \pm 5.9$
2.6444	33.7	46.8 ± 7.9	164.1 ± 16.7	0.160	0.223	1.154	1.039	$55.4 \pm 4.9 \pm 3.6$
2.6464	34.0	51.8 ± 8.3	148.2 ± 17.0	0.160	0.222	1.157	1.039	$52.7 \pm 5.0 \pm 3.8$
2.9000	105.	137.4 ± 13.0	288.7 ± 22.4	0.163	0.211	1.192	1.033	$37.3 \pm 2.2 \pm 2.8$
2.9500	15.9	19.6 ± 4.9	43.2 ± 8.3	0.161	0.203	1.197	1.029	$37.4 \pm 5.7 \pm 2.9$
2.9810	16.1	13.5 ± 4.3	35.5 ± 8.3	0.163	0.206	1.199	1.025	$28.1 \pm 5.2 \pm 2.0$
3.0000	15.9	16.1 ± 4.5	33.8 ± 7.8	0.163	0.204	1.197	1.021	$29.7 \pm 5.3 \pm 2.0$
3.0200	17.3	13.6 ± 4.8	33.9 ± 7.6	0.163	0.204	1.199	1.014	$26.1 \pm 5.0 \pm 2.3$
3.0800	126.	88.0 ± 10.2	218.3 ± 20.1	0.157	0.191	1.135	0.915	$28.0 \pm 2.0 \pm 1.9$

resulting in 1.0% per pion for tracking and 1.0% per pion for PID. The uncertainty on the photon efficiency is estimated as 1.0% per photon by using a control sample of $e^+e^- \rightarrow \pi^+\pi^-\pi^0$ [36]. Since the number of photon for mode I and mode II are two and one respectively, the larger change in the cross section due to shifting the detection efficiency by $\pm 2.0\%$ for mode I and $\pm 1.0\%$ for mode II in the simultaneous fit (with both shifts having the same sign), is taken as the systematic uncertainty.

To estimate the uncertainty of the MC modeling, we examine the efficiency at 2.1250 GeV, which has the largest statistics among all the c.m. energies. The signal MC samples are weighted according to the Dalitz distribution of $e^+e^- \rightarrow \eta'\pi^+\pi^-$ in data after background subtraction. The difference between the weighted efficiency and the nominal efficiency, 1.3%, is taken as the systematic uncertainty. Due to the limited statistics at other c.m. energies, this systematic uncertainty is taken to be the same as that for 2.1250 GeV at all energies.

The track helix parameters for the MC simulation are corrected before the 4C kinematic fit to account for observed data-MC differences [37]. The differences in detection efficiencies with and without corrections, (0.8 – 1.9)%, are assigned as the systematic uncertainty from the 4C kinematic fit.

The uncertainty originating from the ISR correction factor is taken as the relative difference of the values of $(1 + \delta^r) \cdot \epsilon$ between the last two iterations of the cross section measurement.

Three uncertainties associated with the fits to the mass spectra are examined. The background shape is replaced by a third-order Chebychev polynomial function. The signal shape is replaced with a Gaussian function with fixed resolution, obtained by shifting the resolution from the nominal fit by one standard deviation in each direction. Finally, the fit range is varied by ± 5 MeV. The quadrature sum of the changes in the fitted yields is taken as the uncertainty.

The impact of uncertainties on the branching fractions of the intermediate states is examined by changing the branching fractions of η and η' by $\pm 1\sigma$ in the simultaneous fit, where σ is the uncertainty of the individual branching fractions. The difference on the cross section, 1.8%, is taken as the systematic uncertainty.

Adding the systematic uncertainties in quadrature yields the total systematic uncertainties of the measured Born cross sections, which are summarized in Table II.

V. FIT TO THE BORN CROSS SECTION

The obtained Born cross sections are shown in Figure 5 in which a clear structure around 2.05 GeV is observed. To determine the mass and width of the possible resonance, a χ^2 fit is performed to these cross sections. The cross section is parameterized as the coherent sum of a resonant amplitude described by a Breit-Wigner func-

Table II: Systematic uncertainties (in %) from luminosity (\mathcal{L}), photon reconstruction (photon), tracking, PID, MC modeling (MC), kinematic fit (KF), radiation correction (RC), fitting and quoted branching fraction in the cross section measurements. The sources with * superscript are common systematic uncertainties for different c.m. energies.

\sqrt{s} (GeV)	\mathcal{L}^*	photon*	tracking*	PID*	MC*	KF	RC	Fitting	\mathcal{B}^*	Sum
2.0000	1.0	1.3	4.0	4.0	1.3	1.6	0.5	1.7	1.8	6.7
2.0500	1.0	1.3	4.0	4.0	1.3	1.5	0.1	2.3	1.8	6.9
2.1000	1.0	1.3	4.0	4.0	1.3	1.9	0.5	2.5	1.8	7.1
2.1250	1.0	1.3	4.0	4.0	1.3	1.8	0.4	1.2	1.8	6.7
2.1500	1.0	1.3	4.0	4.0	1.3	1.7	0.4	1.7	1.8	6.8
2.1750	1.0	1.3	4.0	4.0	1.3	1.7	0.1	1.3	1.8	6.7
2.2000	1.0	1.3	4.0	4.0	1.3	1.8	0.8	5.4	1.8	8.5
2.2324	1.0	1.3	4.0	4.0	1.3	1.7	0.1	4.9	1.8	8.2
2.3094	1.0	1.3	4.0	4.0	1.3	1.7	0.2	1.8	1.8	6.8
2.3864	1.0	1.3	4.0	4.0	1.3	1.5	0.6	3.2	1.8	7.2
2.3960	1.0	1.3	4.0	4.0	1.3	1.4	0.3	1.3	1.8	6.6
2.6444	1.0	1.3	4.0	4.0	1.3	1.4	0.5	0.7	1.8	6.5
2.6464	1.0	1.3	4.0	4.0	1.3	1.3	0.4	3.3	1.8	7.2
2.9000	1.0	1.3	4.0	4.0	1.3	1.3	0.1	3.9	1.8	7.5
2.9500	1.0	1.3	4.0	4.0	1.3	0.8	0.1	4.2	1.8	7.6
2.9810	1.0	1.3	4.0	4.0	1.3	1.9	0.1	3.0	1.8	7.2
3.0000	1.0	1.3	4.0	4.0	1.3	1.3	0.1	1.9	1.8	6.7
3.0200	1.0	1.3	4.0	4.0	1.3	1.2	0.4	5.8	1.8	8.7
3.0800	1.0	1.3	4.0	4.0	1.3	1.4	0.7	2.3	1.8	6.9

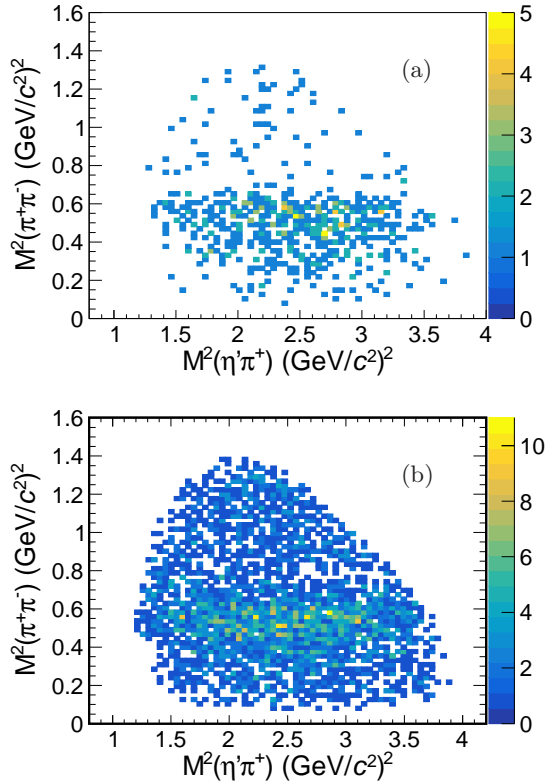


Figure 3: Dalitz plots of the accepted $e^+e^- \rightarrow \eta'\pi^+\pi^-$ candidate events for (a) mode I and (b) mode II in data at $\sqrt{s} = 2.1250$ GeV. The requirement $M(\eta\pi^+\pi^-, \gamma\pi^+\pi^-) \in (0.943, 0.973)$ GeV/ c^2 has been imposed.

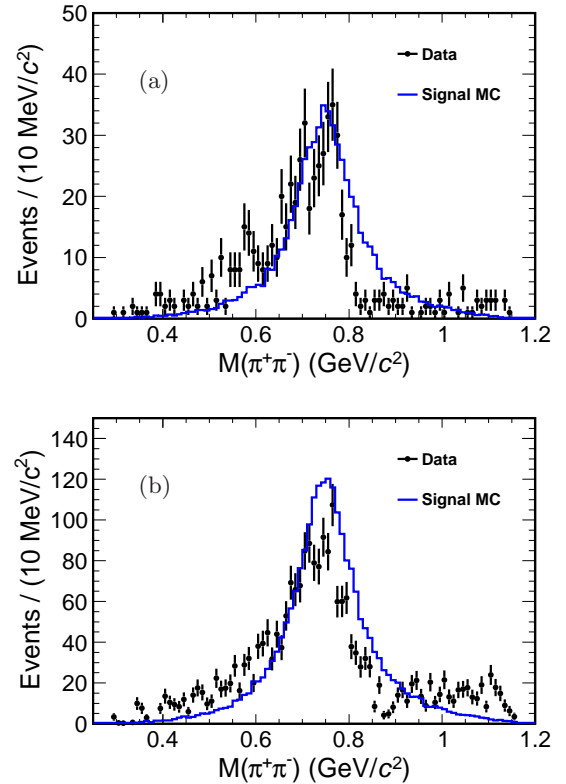


Figure 4: Projections of the corresponding Dalitz plots on $M^2(\pi^+\pi^-)$ axis for (a) mode I and (b) mode II in data (dots with error bars) and signal MC (histograms) at $\sqrt{s} = 2.1250$ GeV.

tion and an s -dependent continuum amplitude [38]:

$$\sigma(s) = \left| \frac{C_0}{s^n} \sqrt{\Phi(\sqrt{s})} + C_1 \cdot BW(\sqrt{s}) \times e^{i\phi} \right|^2, \quad (2)$$

where C_0 and n are the continuum parameters, $C_1 = 3.894 \times 10^5 \text{ nb} \cdot \text{GeV}^2$ is a unit conversion factor, and ϕ is the phase angle between the amplitudes. The relativistic Breit-Wigner amplitude is given by

$$BW(\sqrt{s}) = \frac{\sqrt{12\pi\Gamma_R^{ee}\mathcal{B}_R\Gamma_R^{\text{tot}}}}{s - M_R^2 + iM_R\Gamma_R^{\text{tot}}} \sqrt{\frac{\Phi(\sqrt{s})}{\Phi(M_R)}}, \quad (3)$$

where M_R , Γ_R^{ee} and Γ_R^{tot} are the mass, partial width to e^+e^- and total width of the assumed resonance R . \mathcal{B}_R is the branching fraction for $R \rightarrow \pi^+\pi^-\eta'$, and $\Phi(\sqrt{s})$ is the two-body PHSP factor of $R \rightarrow \rho\eta'$ [1].

In the fit, the correlated and uncorrelated uncertainties are incorporated and the χ^2 is constructed as

$$\chi^2 = \Delta X^T \mathcal{M}^{-1} \Delta X, \quad (4)$$

where ΔX is the difference between the measured and predicted cross sections; the uncertainty of the measured value includes the uncorrelated statistical and systematic components. \mathcal{M} is the covariance matrix; its diagonal elements represent the total uncertainty and off-diagonal elements are correlated systematic uncertainties.

The systematic uncertainties marked with * in Table II are treated as fully correlated uncertainties, while the other systematic uncertainties are considered independent for the various c.m. energies. \mathcal{M} is defined as

$$\mathcal{M}_{i,j} = \sum_k x_i \epsilon_{i,j,k} x_j \epsilon_{j,i,k}, \quad (5)$$

where x_i is the measured value at c.m. energy i , $\epsilon_{i,j,k} = \epsilon_{j,i,k}$ is the common relative systematic uncertainty of x_i and x_j from correlated source k .

Figure 5 shows the result of the fit to the Born cross sections. There are two solutions with equal fit quality and very similar mass and width for the resonance, while the product $\mathcal{B}_R\Gamma_R^{ee}$ and phases are different in the two solutions. The goodness of fit is $\chi^2/\text{n.d.f.} = 9.4/13 = 0.72$, where n.d.f. is the number of degrees of freedom. The fit parameters are summarized in Table III. Since the mass, width, $n(n')$ and $C_0(C'_0)$ values of the two solutions are consistent within 0.2 standard deviation, we present the average values of the two solutions in Table III. The statistical significance of this resonance is estimated to be 6.3σ , by comparing the change of χ^2 ($\Delta\chi^2 = 50.5$), with and without the R amplitude in the fit and taking the change of degrees of freedom ($\Delta\text{n.d.f.}=4$) into account.

The systematic uncertainties of the resonance parameters come from the c.m. energy calibration, the resonance model, the parameterization of the continuum and the type of PHSP factor. The uncertainties of the measured Born cross sections have been included in the fit.

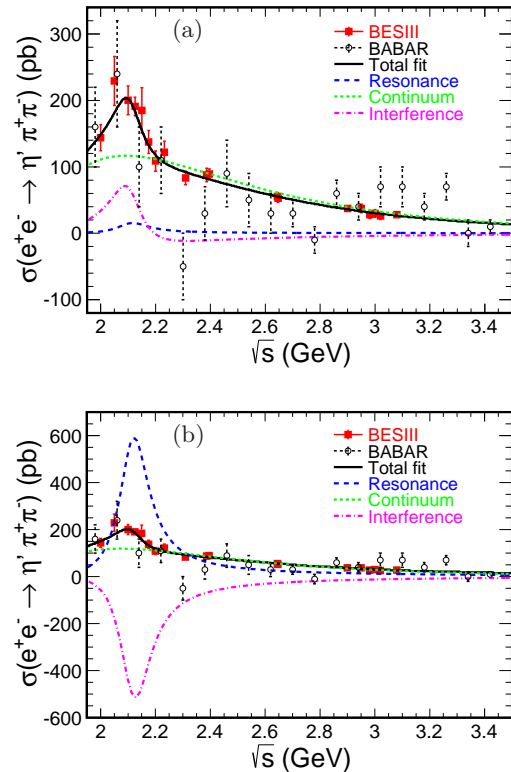


Figure 5: Fit to the $e^+e^- \rightarrow \eta'\pi^+\pi^-$ Born cross sections (only BESIII results). (a) Solution I, constructive interference. (b) Solution II, destructive interference. Red solid dots with error bars are BESIII data, and hollow dots with error bars are BABAR data. The black solid curve is the total fit result, the blue dashed line is the resonant component, the green dashed line is the continuum contribution, and the magenta dot-dashed line represents the interference between the resonance and the continuum contribution. The systematic uncertainties are included.

Table III: Results of the fit to $e^+e^- \rightarrow \eta'\pi^+\pi^-$ Born cross section. The first uncertainties are statistical and the second systematic. n' and C'_0 are parameters of the alternative parameterization of the continuum contribution.

Parameter	Solution 1	Solution 2
M_R (MeV/ c^2)	2111 \pm 43 \pm 25	
Γ_R^{tot} (MeV)	135 \pm 34 \pm 30	
$\mathcal{B}_R\Gamma_R^{ee}$ (eV)	0.64 \pm 0.49 \pm 0.42	23.3 \pm 5.3 \pm 3.3
ϕ (rad)	2.24 \pm 0.73 \pm 0.48	4.46 \pm 0.06 \pm 0.10
$n(n')$	4.42 \pm 0.22 \pm 0.20	(1.66 \pm 0.12 \pm 0.07)
$C_0(C'_0)$	921 \pm 240 \pm 114	(53.0 \pm 13.2 \pm 0.1)

The systematic uncertainty of the c.m. energy is found to be negligible.

To estimate the uncertainty related to the fit model, a modified Breit-Wigner function, in which the width is energy dependent, is employed in the fit. The width of

the modified Breit-Wigner function is written as:

$$\Gamma(\sqrt{s}) = \Gamma_R \left| \frac{p}{p_R} \right|^{2L+1} \frac{M_R}{\sqrt{s}} \frac{B(p)}{B(p_R)}, \quad (6)$$

where Γ_R is the nominal width. p and p_R are the daughter momenta in the rest frame of P , when P taken as \sqrt{s} or M_R , respectively. L is the angular momentum of the decay specified in its subscript. $B(p)$ is the Blatt-Weisskopf form factor [39]. The shifts of the mass and width, which are 14 MeV/ c^2 and 17 MeV, respectively, are taken as the systematic uncertainties.

The uncertainty of the parameterization of the continuum contribution is estimated by replacing C_0/s^n with an exponential function of the form $C'_0 \cdot e^{-n'(\sqrt{s}-M_{th})}$, where $M_{th} = m_\rho + m_{\eta'}$. The differences of the obtained mass and width, which are 21 MeV/ c^2 and 24 MeV, respectively, are assigned as the corresponding systematic uncertainties.

To assess the uncertainty regarding the PHSP factor, we replace the two-body PHSP factor with an alternative PHSP factor consist of 90% two-body and 10% three-body PHSP factor. The resulting changes in the fit of 0.4 MeV/ c^2 for the mass and 4.1 MeV for the width are taken as the systematic uncertainties.

A quadrature sum of all contributions yields total systematic uncertainties for the mass and width of 25 MeV/ c^2 and 30 MeV, respectively.

VI. SUMMARY AND DISCUSSION

We present measurements of the Born cross sections for $e^+e^- \rightarrow \eta'\pi^+\pi^-$ using the data samples collected by the BESIII detector at c.m. energies between 2.00 and 3.08 GeV. The measured Born cross sections are consistent with those of BABAR but have much improved precision. The Born cross section line shape fit has two solutions with equal fit quality and identical mass and width of the resonance, while the product $\mathcal{B}_R\Gamma_R^{e^+e^-}$ and phase are different in the two solutions. The statistical significance of the observed resonant structure is 6.3σ , and its mass, width and $\mathcal{B}_R\Gamma_R^{e^+e^-}$ are determined to be $M = 2111 \pm 43 \pm 25$ MeV/ c^2 , $\Gamma = 135 \pm 34 \pm 30$ MeV and $\mathcal{B}_R\Gamma_R^{e^+e^-} = (0.64 \pm 0.49 \pm 0.42)$ eV or $(23.3 \pm 5.3 \pm 3.3)$ eV, respectively, where the first uncertainties are statistical and the second systematic. The mass and width measured in this work agree with those of the $Y(2040)$ resonance found in $e^+e^- \rightarrow \omega\pi^0$ by BESIII ($M = 2034 \pm 13 \pm 9$ MeV/ c^2 , $\Gamma = 234 \pm 30 \pm 25$ MeV) [17] and with those of the $\rho(2150)$ resonance found in $e^+e^- \rightarrow \eta'\pi^+\pi^-$ by BABAR

($M = 1990 \pm 80$ MeV/ c^2 , $\Gamma = 310 \pm 140$ MeV) [16] within two standard deviation.

The $e^+e^- \rightarrow \pi^+\pi^-\eta'(\eta)$ processes are also studied in the Resonance Chiral Theory framework and the extended Nambu-Jona-Lasinio model [40–44]. However, most of the comparisons of experimental data with those theory predictions are performed in the energy region below 2.0 GeV. With more resonances being included and precise experimental measurements available, these theory models could be tested above 2 GeV in the future.

VII. ACKNOWLEDGMENTS

The BESIII collaboration thanks the staff of BEPCII and the IHEP computing center for their strong support. This work is supported in part by National Key Basic Research Program of China under Contract No. 2015CB856700; National key R & D program of China under Contracts No. 2020YFA0406400 and No. 2020YFA0406300; National Natural Science Foundation of China (NSFC) under Contracts No. 11975118, No. 11625523, No. 11635010, No. 11735014, No. 11822506, No. 11835012, No. 11935015, No. 11935016, No. 11935018 and No. 11961141012, No. 11605196, No. 11605198, No. 11950410506, No. 12061131003, No. 11705192, and No. 12035013; Natural Science Foundation of Hunan Province under Contract No. 2019JJ30019; The Chinese Academy of Sciences (CAS) Large-Scale Scientific Facility Program; Joint Large-Scale Scientific Facility Funds of the NSFC and CAS under Contracts No. U1732263, No. U1832103, No. U1832207, No. U2032111, No. U2032105; CAS Key Research Program of Frontier Sciences under Contracts Nos. QYZDJ-SSW-SLH003, QYZDJ-SSW-SLH040; 100 Talents Program of CAS; INPAC and Shanghai Key Laboratory for Particle Physics and Cosmology; ERC under Contract No. 758462; German Research Foundation DFG under Contracts Nos. 443159800, Collaborative Research Center CRC 1044, FOR 2359, FOR 2359, GRK 214; Istituto Nazionale di Fisica Nucleare, Italy; Ministry of Development of Turkey under Contract No. DPT2006K-120470; National Science and Technology fund; Olle Engkvist Foundation under Contract No. 200-0605; STFC (United Kingdom); The Knut and Alice Wallenberg Foundation (Sweden) under Contract No. 2016.0157; The Royal Society, UK under Contracts Nos. DH140054, DH160214; The Swedish Research Council; U. S. Department of Energy under Contracts Nos. DE-FG02-05ER41374, DE-SC-0012069

[1] P.A. Zyla *et al.* [Particle Data Group], Prog. Theor. Exp. Phys. **2020**, 083C01 (2020).

[2] A. Hasan and D. V. Bugg, Phys. Lett. B **334**, 215 (1994).

- [3] A. V. Anisovich, C. A. Baker, and C. J. Batty, Phys. Lett. B **491**, 47 (2000).
- [4] A. V. Anisovich, C. A. Baker, and C. J. Batty, Phys. Lett. B **508**, 6 (2001).
- [5] A. V. Anisovich, C. A. Baker, and C. J. Batty, Phys. Lett. B **513**, 281 (2001).
- [6] A. V. Anisovich, C. A. Baker, and C. J. Batty, Phys. Lett. B **542**, 8 (2002).
- [7] D.V. Bugg, Phys. Rep. **397**, 257 (2004).
- [8] S. Godfrey and N. Isgur, Phys. Rev. D **32**, 189 (1985).
- [9] D. V. Bugg, Phys. Rev. D **87**, 118501 (2013).
- [10] A. V. Anisovich, V. V. Anisovich, and A. V. Sarantsev, Phys. Rev. D **62**, 051502 (2000).
- [11] P. Masjuan, E. R. Arriola, and W. Broniowski, Phys. Rev. D **85**, 094006 (2012); **87**, 118502 (2013).
- [12] L. P. He, X. Wang, and X. Liu, Phys. Rev. D **88**, 034008 (2013).
- [13] Z. Y. Li, D. M. Li, E. Wang, W. C. Yan, and Q. T. Song, arXiv:2102.05356 [hep-ex].
- [14] M. Atkinson *et al.* [Omega Photon Collaboration], Z. Phys. C **29**, 333 (1985).
- [15] T. H. Bauer, R. D. Spital, D. R. Yennie, and F. M. Pipkin, Rev. Mod. Phys. **50**, 261 (1978).
- [16] B. Aubert *et al.* [BABAR Collaboration], Phys. Rev. D **76**, 092005 (2007); **77**, 119902(E) (2008).
- [17] M. Ablikim *et al.* [BESIII Collaboration], Phys. Lett. B **813**, 136059 (2021).
- [18] C. H. Yu *et al.*, Proceedings of IPAC2016, Busan, Korea, 2016, doi:10.18429/JACoW-IPAC2016-TUYA01.
- [19] M. Ablikim *et al.* [BESIII Collaboration], Nucl. Instrum. Meth. A **614**, 345 (2010).
- [20] M. Ablikim *et al.* [BESIII Collaboration], Chin. Phys. C **44**, 040001 (2020).
- [21] S. Agostinelli *et al.* [GEANT4 Collaboration], Nucl. Instrum. Meth. A **506**, 250 (2003).
- [22] Z. Y. Deng *et al.*, Chin. Phys. C **30**, 371 (2006).
- [23] G. Balossini, C. M. C. Calame, G. Montagna, O. N. F. Piccinini, Nucl. Phys. B **758**, 227 (2006).
- [24] B. Andersson and H. M. Hu, arXiv:hep-ph/9910285.
- [25] M. Ablikim *et al.* [BESIII Collaboration], Chin. Phys. C, **41**, 063001 (2017).
- [26] R. G. Ping, Chin. Phys. C **38**, 083001 (2014).
- [27] G. J. Gounaris and J. J. Sakurai, Phys. Rev. Lett. **21**, 244, (1968).
- [28] M. Ablikim *et al.* [BESIII Collaboration], Phys. Rev. Lett. **120**, 242003 (2018).
- [29] E. A. Kuraev and V. S. Fadin, Yad. Fiz. **41**, 733 (1985)[Sov. J. Nucl. Phys. **41**, 466(1985)].
- [30] S. Actis *et al.*, Eur. Phys. J. C **66**, 585 (2010).
- [31] M. Ablikim *et al.* [BESIII Collaboration], Phys. Rev. D **99**, 032001 (2019).
- [32] M. Ablikim *et al.* [BESIII Collaboration], Phys. Rev. D **100**, 032009 (2019).
- [33] M. Ablikim *et al.* [BESIII Collaboration], Phys. Rev. Lett. **124**, 112001 (2020).
- [34] M. Ablikim *et al.* [BESIII Collaboration], Phys. Rev. D **102**, 012008 (2020).
- [35] M. Ablikim *et al.* [BESIII Collaboration], Chin. Phys. C **41**, 063001 (2017).
- [36] M. Ablikim *et al.* [BESIII Collaboration], Phys. Rev. D **99**, 011101 (2019).
- [37] M. Ablikim *et al.* [BESIII Collaboration], Phys. Rev. D **87**, 012002 (2013).
- [38] C. D. Lü, W. Wang, and Y. M. Wang, Phys. Rev. D **75**, 094020 (2007).
- [39] S. U. Chung, Phys. Rev. D **57**, 431 (1998).
- [40] D. GómezDumm and P. Roig, Phys. Rev. D **86**, 076009 (2012).
- [41] L. Y. Dai, J. Portoles, and O. Shekhovtsova, Phys. Rev. D **88**, 056001 (2013).
- [42] M. K. Volkov, A. B. Arbuzov, and D. G. Kostunin, Phys. Rev. C **89**, 015202 (2014).
- [43] L. Y. Dai, X. W. Kang, Ulf-G. Meibner, X. Y. Song, and D. L. Yao, Phys. Rev. D **97**, 036012 (2018).
- [44] W. Qin, L. Y. Dai, and J. Portoles, JHEP **03**, 092 (2021).